A Global Climatology of Tropospheric and Stratospheric Ozone Derived from Aura OMI and MLS Measurements

Ziemke[1,2], J. R., S. Chandra[2,3], G. Labow[4], P. K. Bhartia[2], L. Froidevaux[5], and J. C. Witte[4]

[1]Goddard Earth and Sciences Technology and Research, Morgan State University, Baltimore, Maryland, USA.
[2]NASA Goddard Space Flight Center, Greenbelt, Maryland, USA.
[3]Goddard Earth Sciences and Technology, University of Maryland Baltimore County, Baltimore, Maryland, USA.
[4]Science Systems and Applications, Inc., Lanham, Maryland, USA.
[5]NASA Jet Propulsion Laboratory, Pasadena, California, USA.

(To be submitted to *Atmos. Chem. Phys.*, June 2011)

Abstract. A global climatology of tropospheric and stratospheric column ozone is derived by combining six years of Aura Ozone Monitoring Instrument (OMI) and Microwave Limb Sounder (MLS) ozone measurements for the period October 2004 through December 2010. The OMI/MLS tropospheric ozone climatology exhibits large temporal and spatial variability which includes ozone accumulation zones in the tropical south Atlantic year-round and in the subtropical Mediterranean/Asia region in summer months. High levels of tropospheric ozone in the northern hemisphere also persist in mid-latitudes over the eastern North American and Asian continents extending eastward over the Pacific Ocean. For stratospheric ozone climatology from MLS, largest ozone abundance lies in the northern hemisphere in the latitude range 70°N-80°N in February-April and in the southern hemisphere around 40°S-50°S during months August-October. The largest stratospheric ozone abundances in the northern hemisphere lie over North America and eastern Asia extending eastward across the Pacific Ocean and in the

31 southern hemisphere south of Australia extending eastward across the dateline. With the
32 advent of many newly developing 3D chemistry and transport models it is advantageous
33 to have such a dataset for evaluating the performance of the models in relation to
34 dynamical and photochemical processes controlling the ozone distributions in the
35 troposphere and stratosphere. The OMI/MLS ozone gridded climatology data, both
36 calculated mean values and RMS uncertainties are made available to the science
37 community via the NASA total ozone mapping spectrometer (TOMS) website http://toms
38 gsfc.nasa.gov.
39
40 **1. Introduction.**
41
42 In a previous paper *Ziemke et al.* [2006] combined ozone measurements from the Ozone
43 Monitoring Instrument (OMI) and Microwave Limb Sounder (MLS) onboard the Aura
44 satellite to obtain global maps of tropospheric column ozone (TCO). The derivation of
45 TCO was based upon a tropospheric ozone residual (TOR) method which involved
46 subtracting MLS stratospheric column ozone (SCO) from OMI total column ozone after
47 adjusting for calibration differences between the two instruments. The TOR concept,
48 which was first applied by *Fishman et al.* [1990] involved measurements of total and
49 stratospheric column ozone from two separate instruments on two separate satellites.
50 Total column ozone was obtained from the Nimbus 7 TOMS UV backscatter instrument
51 while SCO was obtained from Stratospheric Aerosols and Gas Experiment (SAGE)
52 occultation instrument. Aside from calibration issues involving the use of two different
53 satellite measurements, there was also a serious constraint in producing global data with
54 adequate temporal and spatial coverage. Although TOMS total column ozone was daily
55 with near global coverage, SAGE daily SCO measurements were limited to ~30 ozone
56 profiles per day with about one month required to cover the latitude range 50°S-50°N.
57 *Chandra et al.* [2003] later combined total column ozone from Nimbus 7 and Earth Probe
58 TOMS with Upper Atmosphere Research Satellite (UARS) MLS ozone measurements to
59 derive improved measurements of TCO extending from the tropics to the extra-tropics;
60 that study was the first to use MLS ozone measurements to derive a long record of TCO
61 spanning ~6 years. Having essentially coincident measurements along each orbital track

with current Aura OMI and MLS column ozone is a significant improvement from these previous studies in the ability to produce global maps of TCO from daily to longer timescales.

The study by *Ziemke et al.* [2006] used 2D interpolation of MLS to derive fields of SCO prior to deriving TCO. This method involved first applying a moving Gaussian interpolation to fill in missing MLS measurements along each daytime orbital track (on average about 14.6 south-to-north orbital tracks per day) followed by linear interpolation along longitude. This simple interpolation scheme for deriving daily gridded SCO fields works well provided that horizontal gradients in SCO are small. Meaningful daily maps of SCO can be determined from 2D interpolation excluding regions of polar night and the tropospheric wind jets. Other methods have been introduced for obtaining daily maps of SCO and TCO. *Schoeberl et al.* [2007] introduced a wind trajectory scheme using MLS ozone profiles and showed improvements for daily SCO and TCO in the extra-tropics. More recently *Liu et al.* [2010] describes an OMI-only ozone profile retrieval algorithm to derive daily fields of TCO and SCO. Other methods include data assimilation such as from the NASA Global Modeling and Assimilation Office (GMAO) [*Stajner, et al.*, 2008] and also Aura TES ozone profile measurements [*Zhang et al.*, 2010].

All of these methods including simple 2D interpolation appear to do well in deriving global SCO and TCO for monthly averages, but accurate daily measurements remain generally constrained to excluding the wind jet regions. Even for regions where SCO does not vary appreciably, it remains to be shown that invoking more sophisticated methods beyond simple interpolation are an improvement because of potential induction of additional sources of error such as from assimilated wind fields or other ancillary data input to the algorithm. *Tan et al.* [2004] has shown that assimilated winds in the stratosphere have substantial errors caused by over-determination of mixing and entrainment rates in subtropical latitudes. Because of this, for a relatively long-lived constituent such as ozone in the lower stratosphere these errors propagate to errors in the tropical SCO field. It remains to be shown which of the various methods can provide

92 adequate accuracy and precision of SCO and TCO in the dynamical wind jet regions to
93 derive true daily global maps (this is current collaborative work in progress).
94
95 The objective of this study is to develop a six-year global climatology of TCO and SCO
96 from Aura OMI and MLS measurements. The importance of such a dataset is two-fold:
97 (1) The dataset is useful as a benchmark test of basic seasonal-cycle and seasonal spatial
98 variability present in photochemistry-transport models of tropospheric and stratospheric
99 ozone, and also evaluating ozone precursors, and (2) the OMI/MLS dataset is also
100 potentially useful as a priori information for ozone retrieval algorithms. It is noted that
101 *Martin et al.* [2007] included an earlier version of OMI/MLS monthly mean TCO and
102 derived an optimal assessment of global tropospheric nitrogen in the Goddard Earth
103 Observing System Chemistry-transport model (GEOS-Chem) which was consistent with
104 both the OMI/MLS ozone and the generated modeled ozone. In other words, by varying
105 nitrogen in the model it was possible to yield consistent TCO between measurement and
106 model, thus improving confidence in the assessed modeled nitrogen.
107
108 In the following, section 2 discusses the OMI and MLS satellite measurements, section 3
109 compares the TCO with ozonesondes, sections 4 and 5 discusses TCO and SCO
110 climatologies from OMI/MLS, and finally section 6 is a summary.
111
112 **2. Aura OMI and MLS Ozone Measurements.**
113
114 OMI and MLS are two out of a total of four instruments onboard the Aura spacecraft
115 which is flown in a sun-synchronous polar orbit at 705 km altitude with a 98.2^{o}
116 inclination. Aura was launched in July 2004 and has been providing data measurements
117 since August 2004 to the present. The spacecraft has an equatorial crossing time of 1:45
118 pm (ascending node) with around 98.8 minutes per orbit (14.6 orbits per day on average).
119 *Schoeberl et al.* [2006] provide an overview of the EOS Aura mission and discuss the
120 various measurements from the four Aura instruments.
121

OMI is a nadir-scanner which at visible (350-500 nm) and UV wavelength channels (UV-1: 270-314 nm; UV-2: 306-380 nm) detects backscattered solar radiance to measure column ozone with near global coverage (aside from polar night latitudes) over the Earth with a resolution of 13 km × 24 km at absolute nadir. Aside from ozone, OMI also measures Optical Centroid Cloud Pressure (OCCP), aerosols, NO_2, SO_2, HCHO, and several other trace gases in the troposphere and stratosphere [*Levelt et al.*, 2006]. Measurements of ozone from OMI are determined using the OMTO3 v8.5 algorithm which is an extension of the TOMS v8 algorithm. A description of the TOMS v8 algorithm may be obtained from the TOMS V8 CD DVD, or from the OMI Algorithm Theoretical Basis Document (ATBD) from the TOMS web page http://toms.gsfc.nasa.gov/version8/v8toms_atbd.pdf). One main difference between the TOMS v8 and the OMTO3 v8.5 algorithms is the treatment of clouds. The TOMS v8 and earlier versions of OMTO3 use a cloud pressure climatology based on thermal infrared cloud-top pressures, whereas OMTO3 v8.5 uses OCCP derived with OMI by the rotational Raman scattering method. The use of simultaneously measured OCCP significantly improves estimates of total column ozone, especially in the presence of bright clouds [*Joiner and Vasilkov*, 2006]. The OMI instrument began having scan measurement errors beginning in year 2007 which are called row anomalies. The OMI instrument has 60 scan rows per orbit path and currently about 1/3 of the scan row measurements are affected. This problem is caused by partial blockage from material in the optical field of OMI but has not degraded appreciably since January 2009.

SCO is calculated for the OMI/MLS residual method using MLS v3.3 ozone profile measurements. The MLS instrument is a thermal-emission microwave limb sounder that measures vertical profiles of mesospheric, stratospheric, and upper tropospheric temperature, ozone, and several other important constituents such as CO and H_2O from limb scans taken in the direction ahead of the Aura satellite orbital track. The MLS profile measurements are made about 7 minutes before OMI views the same location during ascending (daytime) orbital tracks. These we refer to as "co-located" measurements between OMI and MLS. MLS also measures ozone and other atmospheric constituents for descending nighttime orbits which on a given day can be up to ±12 hours

different in time from OMI daytime measurements. With combined ascending and descending nodes MLS makes around 3500 vertical profile measurements over the Earth per day. This study includes only the ascending orbit co-located data from MLS for deriving SCO. Details regarding the instrument including spectrometers, spectral channels, calibration, and other topics are discussed by *Waters et al.* [2006] and in related papers in the same journal. *Froidevaux et al.* [2008] provides validation results for MLS v2.2 measurements of ozone and other trace gases. At the present time both v2.2 and v3.3 are provided to the science community. While v2.2 retrieval has 37 pressure levels, v3.3 has 55 pressure levels and other improvements; however, v3.3 also has more outliers and missing data in the ozone profile measurements than with v2.2. Our analysis of SCO from MLS shows that there is little difference between using v2.2 or v3.3 other than a small systematic offset (v3.3 minus v2.2) at all latitudes of about +2.5 DU. As was similarly done by *Ziemke et al.* [2006], MLS v3.3 SCO was adjusted to CCD SCO from OMI by subtracting this offset from MLS SCO. Information regarding the MLS v3.3 ozone measurements including a data quality description document is available online from the NASA Data and Information Services Center webpage (http://disc.sci.gsfc.nasa.gov/gesNews/mls_new_data_version_release).

For the OMI/MLS residual method SCO is determined from vertically integrated MLS ozone profiles which is subtracted from OMI total column ozone to derive TCO. Tropopause pressure, which separates tropospheric from stratospheric column ozone comes from National Centers for Environmental Prediction (NCEP) using the World Meteorological Organization (WMO) 2K-km^{-1} lapse rate tropopause definition. SCO from MLS is determined by pressure integration of ozone volume mixing ratio profiles from 0.0215 hPa down to the NCEP tropopause. The MLS ozone profile measurements were linearly interpolated in log-pressure to the NCEP tropopause pressure to derive SCO. MLS SCO (in Dobson Units, DU; 1 DU = 2.69×10^{20} molecules-m^{-2}) was determined by standard log-pressure integration of ozone partial pressure: $\mathrm{SCO} = 0.79 \int_{0.0215hPa}^{Ptropopause} XP \cdot d\ln P$, where X is ozone volume mixing ratio in units ppbv and P is pressure in units hPa. The recommended range for scientific analysis of MLS

183 v3.3 ozone profiles is 0.0215-261 hPa. As was done by *Ziemke et al.* [2006], nearly
184 global SCO from MLS for each day was achieved by including ozone retrievals down to
185 316 hPa. The uncertainty in derived SCO from MLS by including the 316 hPa level
186 beyond 261 hPa can be estimated. Documentation for MLS v3.3 ozone measurements
187 suggests RMS uncertainties of about 0.03 ppmv at 261 hPa and 0.05 ppmv at 316 hPa.
188 Using the above integration formula, an upper-bound estimate of the RMS uncertainty in
189 261-316 hPa column ozone from MLS is then about 3.5 DU.

190 MLS SCO data were initially binned to 1^{o} latitude × 1.25^{o} longitude to be compatible
191 with OMI level-3 (L3) gridded total column ozone. Tropopause pressures from NCEP
192 analyses were re-binned to this same resolution from a coarser $2.5^{o} \times 2.5^{o}$ gridding. It is
193 noted for MLS limb measurements that the horizontal optical path is about 300 km which
194 is larger than the horizontal size of OMI L3 gridded data, but is comparable to the size of
195 original NCEP gridded measurements. To derive a high density SCO field we have used
196 the two-step spatial interpolation of *Ziemke et al.* [2006]. The interpolation for SCO
197 includes first a moving 2D (latitude/longitude) Gaussian window along daytime orbit to
198 fill in intermittent gaps along-track for MLS SCO, followed secondly by a linear
199 interpolation along longitude between MLS SCO data. This interpolation approach
200 preserves the along-track measurements of SCO from MLS at all latitudes. NCEP
201 measurements of tropopause pressure were re-binned to the same 1^{o} latitude × 1.25^{o}
202 longitude resolution. Following derivation of daily maps of SCO and TCO at $1^{o} \times 1.25^{o}$
203 resolution, the data were averaged monthly in $5^{o} \times 5^{o}$ and $10^{o} \times 10^{o}$ bins. We have
204 evaluated OMI and MLS ozone data for the time period 1 October 2004 – 31 December
205 2010 which represents approximately six years of continuous measurements. The TCO
206 and SCO monthly climatology fields were smoothed along longitude using Fourier
207 analysis by retaining zonal wave numbers 0-12 which both reduces noise and ensures
208 periodic continuation across the dateline.
209
210 **3. Comparisons of OMI/MLS Tropospheric Ozone with Ozonesondes.**
211

212 Validation of OMI/MLS TCO is based upon Southern Hemisphere Additional
213 OZonseondes (SHADOZ) and World Ozone and Ultraviolet radiation Data Center
214 (WOUDC) ozonesonde measurements whereby monthly means from OMI/MLS are
215 compared with monthly ensemble averages from the ozonesondes. The ozonesonde data
216 represent for each station an average of all existing ozonesonde measurements in a given
217 month (which could vary from one to several). OMI/MLS TCO was converted to ozone
218 mean volume mixing ratio and then compared with mean volume mixing ratio for both
219 the SHADOZ and WOUDC ozonesondes. Ozone mean volume mixing ratio for the
220 tropical SHADOZ stations involved pressure averaging of ozone for ground-to-120 hPa
221 while for extra-tropical WOUDC stations this was ground-to-350 hPa. The ozonesonde
222 data for our comparisons extend for years 2004-2009 for SHADOZ and 2005-2008 for
223 WOUDC. Of the several SHADOZ and WOUDC stations processed, 39 of them had
224 measurements that overlapped with the OMI/MLS time period.
225
226 Figure 1 and Figure 2 show tropospheric ozone time series comparisons for several
227 stations from SHADOZ and WOUDC, respectively. Also included in these figures are 1-
228 1 scatter diagrams of the combined data. The stations in Figures 1 and 2 were chosen not
229 just because these are common stations but also because of large annual-cycle variability
230 (20-30 ppbv peak-to-peak) with nearly complete month-to-month temporal coverage.
231
232 There are important issues involved when comparing ozonesondes with satellite ozone
233 measurements. Balloon ozonesondes represent wind advected measurements along
234 trajectory paths and are very different than the satellite measurements which provide
235 ozone averages over broad regions. Also, ozone in the troposphere (such as shown by
236 *Avery et al.* [2010]) exhibits large changes of 30-50 ppbv over horizontal distances of
237 only a few km or less. With such enormous spatial variability the most one can gain in
238 comparing satellite measured ozone versus ozonesondes is to evaluate seasonal
239 variability and climatological means, and extreme cases such as inter-annual variability
240 events in the tropical Pacific caused by ENSO. Table 1 provides a list of comparisons
241 between OMI/MLS and the SHADOZ/WOUDC ozonesondes with station latitudes
242 arranged from northern-most at top to southern-most at bottom. Listed for each station is

243 the total number of daily profile measurements, mean values for OMI/MLS and
244 ozonesondes, and standard RMS of their differences. For most of the stations listed in
245 Table 1 the RMS values lie between 4 ppbv and 10 ppbv. For stations northward of 50°N,
246 RMS is greater than 10 ppbv except for Debilt and Valentia. The larger RMS numbers in
247 NH high latitudes are partly explained by the sparse nature of monthly measurements
248 from both OMI/MLS and ozonesondes. Figure 3 compares climatological means for
249 OMI/MLS and ozonesondes. The left panel in Figure 3 represents station latitudes 25°S-
250 50°N and the right panel is the same but includes stations pole ward of 50°N.
251
252 **4. Comparisons of OMI/MLS and LLM Tropospheric Ozone Climatology.**
253
254 *Logan* [1999] provided an extensive analysis of global ozone based upon ozonesonde
255 measurements. More recently *McPeters et al.* [2007] expanded the ozonesonde
256 evaluation of *Logan* [1999] and derived a global zonal mean climatology of total
257 atmospheric ozone as a function of latitude, altitude, and month of year. This
258 climatology was determined by combining ozonesondes with satellite ozone
259 measurements from SAGE and MLS. The final climatology product is referred to as the
260 Labow-Logan-McPeters (LLM) climatology and is currently used in the OMTO3 v8.5
261 algorithm processing for both OMI and TOMS ozone retrievals.
262
263 Figure 4 shows a comparison of LLM TCO climatology (top panel) with OMI/MLS TCO
264 climatology (middle panel) and their difference (bottom panel). Fundamental
265 characteristics are generally consistent between the datasets regarding seasonal cycles
266 including the transition in peak TCO in the NH from tropics to mid-latitudes when going
267 from spring to summer months. LLM minus OMI/MLS TCO difference is larger by
268 several DU to more than +5 DU for some months and latitudes in the subtropics and mid-
269 latitudes. These differences are largely explained as an ozonesonde station location issue
270 as the LLM climatology is determined from TCO measurements over land whereas TCO
271 from OMI/MLS in Figure 4 is averaged along all longitudes.
272

That is, because TCO over ocean is generally smaller than over land (as discussed later for Figure 5), OMI/MLS zonal mean TCO will be smaller than LLM TCO. In contrast, in the high latitudes of both hemispheres in Figure 4 the offset differences are instead negative exceeding -5 DU. These differences in the higher latitudes may be explained by both a sparse number of ozonesonde measurements and also high solar-zenith angles which can produce substantial errors in the OMI and/or MLS ozone retrievals.

5. OMI/MLS Global TCO Climatology Maps.

The first study to derive a global TCO climatology maps from satellite measurements was *Fishman et al.* [1990]. As noted in the Introduction, tropospheric ozone determined from TOMS/SAGE residual was limited both temporally and spatially because of sparse SAGE ozone profile measurements. An improvement was made for the SAGE sampling problem by *Fishman et al.* [2003] by using instead NOAA SBUV to derive SCO, however there is little ozone profile information obtained from SBUV below the ozone number density peak (i.e., atmospheric pressures greater than ~30-40 hPa). To alleviate this SBUV ozone profile problem *Fishman et al.* [2003] applied an empirical correction to SBUV ozone profiles to improve the SCO fields. It is anticipated that the use of Aura MLS ozone profile measurements which extend down to 261 hPa for v3.3 substantially improves global climatology estimates of SCO and also TCO.

A six-year TCO climatology from OMI and MLS ozone is shown in Figure 5(a-c) for each of the months January-December. Figure 5 for illustration plots the $10^{o}\times10^{o}$ dataset. TCO in high latitudes is flagged as missing, both for obvious reason involving polar night latitudes (i.e., where there are no OMI measurements) and additional subjective data flagging. Subjective data flagging included OMI scenes with solar zenith angles greater than 82^{o} or questionable derived TCO product values in high latitudes.

The main features of the TCO climatology in Figure 5 are briefly summarized. In tropical latitudes TCO for each month is characterized by low amounts in the Pacific ~15-20 DU with much higher columns ~35-45 DU in the Atlantic. Lowest TCO in the

304 tropics lies in the western Pacific in July-September with numbers less than 15 DU.
305 These low columns are largely a manifestation of deep convection and vertical injection
306 of low marine boundary layer/low tropospheric ozone into the middle and upper
307 troposphere. The highest TCO in the tropics occurs in September-October in the
308 southern Atlantic region extending eastward toward Australia with numbers 40-45 DU.
309 These annually recurring high values in the southern hemisphere are associated with
310 planetary-scale transport of ozone rich air mass and ozone sources including effects from
311 STE and biomass burning. TCO in the northern hemisphere has large topographic
312 variability year-round, with largest columns occurring around May-July over the eastern
313 US eastward over the Atlantic Ocean toward Europe, Mediterranean/western Asia, and
314 eastern Asia extending eastward over the Pacific Ocean toward North America.
315
316 Figure 6 shows line plots of TCO as a function of longitude for 30^{o}-40^{o}N and 0^{o}-10^{o}S.
317 These latitude bands and months were chosen to show several large annually recurring
318 features present in global TCO. The line plots in Figure 6 also include $\pm 2\sigma$ uncertainties
319 for illustration where σ is calculated standard RMS error of the mean. TCO in these two
320 latitude bands has large spatial variability. The left panel shows zonal variability caused
321 by a Mediterranean-Asian accumulation region (centered about 30^{o}E) and the mountains
322 of the Tibetan Plateau (centered about 90^{o}E). The right panel shows large contrast in
323 TCO from low values in the tropical Pacific and high values in the tropical Atlantic (i.e.,
324 about 20 DU versus 40 DU, respectively). The $5^{o}\times5^{o}$ and $10^{o}\times10^{o}$ monthly TCO
325 climatology fields along with their RMS uncertainty fields can be obtained via link from
326 the TOMS webpage (http://toms.gsfc.nasa.gov).
327
328 For applications such as evaluating 3D chemistry-transport models of the atmosphere it is
329 useful to derive a zonal mean climatology of TCO from OMI/MLS. A simple model
330 comparison with zonal mean TCO climatology can reveal fundamental offsets or annual-
331 cycle differences that can be used to aid in the development of models. *Ziemke et al.*
332 [2006] compared an earlier version of zonal mean TCO between OMI/MLS and the
333 Global Modeling Initiative (GMI) 3D model and showed good agreement in latitude
334 gradients and temporal variability except for a 5-10 DU offset in the NH extending from

335 the subtropics out to mid-latitudes. It was surmised that errors in OMI from aerosols
336 could be a contributing factor for the offset, but the primarily indication was that the
337 model was over-determining TCO by several DU in the NH subtropics/mid-latitudes in
338 most months. Figure 7 shows the six-year climatology of zonal mean TCO. Lowest
339 TCO occurs in the SH tropics around 10°S around January-April (<24 DU) and also in
340 the NH and SH mid-latitudes around late fall to winter-spring (<30 DU). Largest TCO
341 occurs in the NH mid-latitudes in June-July (>42 DU) and in the SH subtropics during
342 September-November (>39 DU). There is a transition in the NH from peak values in
343 spring months (March-May) in the tropics/subtropics to peak values in summer (June-
344 July) in the mid-latitudes. This pattern shift from spring to summer with latitude is
345 caused largely by a coupling of spring-summer STE with ozone produced from pollution
346 events in summer months. It is noted that the GMI model evaluated by *Ziemke et al.*
347 [2006] showed all the basic temporal and spatial features in Figure 7 despite an offset
348 difference in the NH mid-latitudes.
349
350 **6. MLS Global SCO Climatology Maps.**
351
352 An SCO climatology from MLS is shown in Figure 8(a-c) for each of the months
353 January-December. As in Figure 4 the data binning is at $10^{o}\times10^{o}$ resolution which for
354 SCO provides nearly global coverage out to central latitudes $\pm85^{o}$. The main features
355 include a contrast between small zonal variability of SCO in the tropics and large
356 planetary-scale variability in the middle and high latitudes in both hemispheres. SCO in
357 Figure 8 should be interpreted carefully in the middle and high latitudes particular to
358 these years 2004-2010 since SCO patterns in both hemispheres can exhibit substantial
359 inter-annual differences in zonal variability caused by stratospheric sudden warming
360 events and the morphology of the breakup of the middle atmosphere polar vortex in the
361 NH and SH. Zonal mean SCO from MLS is shown in Figure 9. SCO in Figure 9 is
362 largest in spring months in both hemispheres. In the Northern hemisphere SCO is largest
363 around February-March at high latitudes and in the Northern Hemisphere SCO is largest
364 around September-October in mid-latitudes. The maximum SCO in the NH occurs in
365 conjunction with high ozone over the central Asian continent extending eastward across

366 North America as shown in Figure 7a. SCO in the SH maximizes equator-ward of the
367 polar vortex in September-October and as Figure 7c shows, originates primarily from the
368 Pacific about the dateline. Table 3 shows the calculated zonal mean SCO climatology
369 values given in 5° latitude bands.
370
371 **7. Summary.**
372
373 A six-year global climatology of tropospheric column ozone (TCO) and stratospheric
374 column ozone (SCO) is derived from combining Aura OMI and MLS measurements for
375 the period October 2004-December 2010. The climatology is useful for several purposes
376 including evaluation of 3D chemistry-transport models and self-generating global
377 circulation models of the atmosphere to assess model performance. By comparing basic
378 seasonal cycles and seasonally-varying spatial variability in TCO and SCO in models
379 with the climatology one can identify and correct problems in models regarding errors in
380 wind fields or invoked photochemical reactions/rates, and errors in emissions including
381 ozone precursors. Another useful application for the global climatology of TCO and
382 SCO includes producing a climatology of radiative forcing coming from upper and lower
383 atmospheric ozone. The total column ozone climatology determined from adding
384 together SCO and clear-sky TCO can also generate a global clear-sky surface UV
385 climatology as a function of region and time of year.
386
387 Algorithms for retrieving ozone such as from remote sensing satellite instruments rely on
388 assumed a priori information of the ozone concentrations. The current OMTO3
389 algorithm invokes the Labow-Logan-McPeters (LLM) zonal mean ozone climatology
390 [*McPeters, et al.*, 2007] which is determined by combining ozonesondes with SAGE and
391 Aura MLS ozone profile measurements. The LLM climatology is given as a function of
392 month, latitude, and altitude. A future task is to combine the LLM and the OMI/MLS
393 climatology products to generate a single 3D (latitude, longitude, altitude) 12-month
394 climatology.
395

396 The TCO and SCO climatology data from OMI/MLS are provided to the community in
397 ASCII formatted tables with IDL and Fortran readers as a link from the TOMS homepage
398 (http://toms.gsfc.nasa.gov). The measurements along with their computed RMS
399 uncertainties are given in these tables at $5^{o} \times 5^{o}$ and $10^{o} \times 10^{o}$ (latitude × longitude)
400 resolution.
401
402 **Acknowledgments.** The authors thank the Aura MLS and OMI instrument and
403 algorithm teams for the extensive satellite measurements used in this study. OMI is a
404 Dutch-Finnish contribution to the Aura mission. Funding for this research was provided
405 in part by NASA NNH07ZDA001N-AST.

406
407 **References.**
408
409 Avery, M., C. Twohy, D. McCabe, et al., Convective distribution of tropospheric ozone
410 and tracers in the Central American ITCZ region: Evidence from observations during
411 TC4, *J. Geophys. Res., 115*, doi:10.1029/2009JD013450, 2010.
412
413 Chandra, S., J. R. Ziemke, and R. V. Martin, Tropospheric ozone at tropical and middle
414 latitudes derived from TOMS/MLS residual: Comparison with a global model, *J.*
415 *Geophys. Res., 108*(D9) doi:10.1029/2002JD002912, 2003.
416
417 Fishman, J., C. E. Watson, J. C. Larsen, and J. A. Logan, Distribution of tropospheric
418 ozone determined from satellite data, *J. Geophys. Res., 95*, 3599-3617, 1990.
419
420 Fishman, J., A. E. Wozniak, and J. K. Creilson, Global distribution of tropospheric ozone
421 from satellite measurements using the empirically corrected tropospheric ozone residual
422 technique: Identification of the regional aspects of air pollution, *Atmos. Chem. Phys.*, 3,
423 893-907, 2003.
424

425 Froidevaux, L., Y. B. Jiang, A. Lambert, et al., Validation of Aura Microwave Limb
426 Sounder stratospheric ozone measurements, *J. Geophys. Res., 113*, D15S20,
427 doi:10.1029/2007JD008771, 2008.
428
429 Joiner, J., and A. P. Vasilkov, First results from the OMI Rotational Raman Scattering
430 Cloud Pressure Algorithm, IEEE T. *Geosci. Remote, 44*, 12721282, 2006.
431
432 Levelt, P. F., et al., Science objectives of the Ozone Monitoring Instrument, *IEEE Trans.*
433 *Geophys. Remote Sens. 44*(5), 1199-1208, 2006.
434
435 Liu, X., P. K. Bhartia, K. Chance, et al., Ozone profile retrievals from the Ozone
436 Monitoring Instrument, *Atmos. Chem. Phys., 10*, 2521-2537, 2010.
437
438 Logan, J. A., An analysis of ozonesonde data for the troposphere: Recommendations for
439 testing 3-D models, and development of a gridded climatology for tropospheric ozone, *J.*
440 *Geophys. Res., 104*, 16,115-16,149, 1999.
441
442 Martin, R. V., B. Sauvage, I. Folkins, C. E. Sioris, C. Boone, P. Bernath, and J. Ziemke,
443 Space-based constraints on the production of nitric oxide by lightning, *J. Geophys. Res.,*
444 *112*, D09309, doi:10.1029/2006JD007831, 2007.
445
446 McPeters, R. D., G. J. Labow, and J. A. Logan, Ozone climatological profiles for satellite
447 retrieval algorithms, *J. Geophys. Res., 112*, D05308, doi:10.1029/2005JD006823, 2007.
448
449 Schoeberl, M. R., et al., Overview of the EOS Aura mission, *IEEE Trans. Geophys. Rem.*
450 *Sens., 44*(5), 1066-1074, 2006.
451
452 Schoeberl, M. R., J. R. Ziemke, B. Bojkov, N. Livesy, B. Duncan, et al., A trajectory-
453 based estimate of the tropospheric ozone column using the residual method, J. Geophys.
454 Res., 112, D24S49, doi:10.1029/2007JD008773, 2007.
455

Stajner, I., K. Wargan, S. Pawson, Assimilated ozone from EOS-Aura: Evaluation of the tropopause region and tropospheric columns, *J. Geophys. Res., 113*, D16S32, doi:10.1029/2007JD008863, 2008.

Tan, W. W., M. A. Geller, S. Pawson, et al., A case study of excessive subtropical transport in the stratosphere of a data assimilation system, *J. Geophys. Res., 109*, D11102, doi:10.1029/2003JD004057, 2004.

Waters, J., et al., The Earth Observing System Microwave Limb Sounder (EOS MLS) on the Aura satellite, *IEEE Trans. Geophys. Remote Sens., 44*(5), 1075-1092, 2006.

Zhang, L., D. J. Jacob, X. Liu, et al., Inter-comparison methods for satellite measurements of atmospheric composition: application to tropospheric ozone from TES and OMI, *Atmos. Chem. Phys., 10*, 4725-4739, doi:10.5194/acp-10-4725-2010, 2010.

Ziemke, J. R., S. Chandra, B. N. Duncan, et al., Tropospheric ozone determined from Aura OMI and MLS: Evaluation of measurements and comparison with the Global Modeling Initiative's Chemical Transport Model, *J. Geophys. Res., 111*, D19303, doi:10.1029/2006JD007089, 2006.

Table and Figure captions

Table 1. Statistical comparisons between OMI/MLS and SHADOZ/WOUDC sonde tropospheric mean volume mixing ratio (in ppbv) with the station latitudes arranged from northern-most at top to southern-most at bottom. Included for each station is the total number of daily profile measurements, mean values for OMI/MLS and ozonesondes, and standard RMS of their differences.

Table 2. Tropospheric column ozone zonal mean climatology (in Dobson Units) from OMI/MLS at 5° latitude resolution.

Table 3. Global stratospheric column ozone zonal mean climatology (in Dobson Units) derived from MLS integrated ozone profiles at 5° latitude resolution.

Figure 1. Comparison time series of tropospheric ozone mean volume mixing ratio (in ppbv) between OMI/MLS (dark curves) and several selected common station measurements from SHADOZ (light curves). Also included at far right is a 1-1 comparison scatter plot for the measurements.

Figure 2. Similar to Figure 1 but for selected extra-tropical WOUDC ozonesonde stations.

Figure 3. (left) Scatter plots of ozonesonde versus OMI/MLS mean tropospheric ozone for ozonesonde station locations lying between 25°S and 50°N. (right) Same as left panel, except for extended latitude range 25°S to 90°N. The values plotted are time series averages in units ppbv.

Figure 4. (top) Labow-Logan_McPeters (LLM) tropospheric column ozone climatology. (middle) OMI/MLS tropospheric column ozone climatology. (bottom) LLM minus OMI/MLS climatology difference. All measurements are in Dobson Units. The colors in the panels going from blue/black to red represent smallest to largest (or most positive) values, respectively.

Figure 5a. Tropospheric column ozone climatology (in Dobson Units) for months January-April from OMI/MLS residual ozone measurements. The colors in the panels going from blue to red represent smallest to largest values, respectively.

Figure 5b. Same as Figure 5a but for months May-August.

Figure 5c. Same as Figure 5b but for months September-December.

518 **Figure 6.** Line plots of tropospheric column ozone (in Dobson Units) as a function of
519 longitude for the latitude bands 30°-40°N and 0°-10°S. The plots include ±2σ
520 uncertainties for illustration where σ is the calculated standard RMS error of the mean.
521
522 **Figure 7.** Zonal mean climatology of tropospheric column ozone (in Dobson Units)
523 derived from October 2004 – December 2010 OMI/MLS at 5° latitude resolution. The
524 shading going from dark to light represents smallest to largest values, respectively.
525
526 **Figure 8a.** Similar to Figure 5a but for stratospheric column ozone (in Dobson Units).
527 The colors in the panels going from blue to red represent smallest to largest values,
528 respectively.
529
530 **Figure 8b**. Similar to Figure 5b but for stratospheric column ozone (in Dobson Units).
531
532 **Figure 8c.** Similar to Figure 5c but for stratospheric column ozone (in Dobson Units).
533
534 **Figure 9.** Zonal mean climatology of stratospheric column ozone (in Dobson Units)
535 from October 2004 – December 2010 MLS at 5° latitude resolution. The shading going
536 from dark to light represents smallest to largest values, respectively.
537
538
539 **Tables**
540
541 **Table 1.** Statistical comparisons between OMI/MLS and SHADOZ/WOUDC sonde
542 tropospheric mean volume mixing ratio (in ppbv) with the station latitudes arranged from
543 northern-most at top to southern-most at bottom. Included for each station is the total
544 number of daily profile measurements, mean values for OMI/MLS and ozonesondes, and
545 standard RMS of their differences.
546

Station	N	OMI/MLS	Sonde	Diff RMS
Alert(82.5N,62.3W)	27	60.2	49.4	19.4
Eureka(80.0N,85.9W)	22	56.9	50.5	13.3

Resolute(74.7N,95.0W)	33	61.9	49.7	19.1
Neumayer(70.7S,8.3W)	26	38.4	30.8	17.7
Lerwick(60.1N,1.2W)	46	57.2	55.2	10.7
Churchill(58.7N,94.1W)	36	61.1	50.6	14.3
Stonyplain(53.6N,114.1W)	45	53.1	48.2	11.0
Goosebay(53.3N,60.4W)	38	57.9	51.4	13.2
Legionwo(52.4N,21.0E)	39	51.8	56.5	12.1
Lindenberg(52.2N,14.1E)	48	51.0	55.9	11.1
Debilt(52.1N,5.2E)	45	52.1	54.7	8.4
Valentia(51.9N,10.3W)	27	56.0	58.0	9.4
Brattslake(50.2N,104.7W)	46	51.9	51.4	12.3
Praha(50.0N,14.5E)	12	50.4	54.1	7.9
Kelowna(49.9N,119.4W)	36	51.1	51.8	12.4
Payerne(46.8N,7.0E)	48	51.7	52.2	6.6
Egbert(44.2N,79.8W)	41	58.3	57.8	9.3
Barajas(40.5N,3.6W)	47	55.9	53.9	7.0
Boulder(40.3N,105.2W)	36	54.0	56.0	6.6
Ankara(40.0N,32.9E)	43	57.5	59.2	9.9
Wallops(37.9N,75.5W)	48	58.6	59.2	6.9
Huntsville(34.7N,86.6W)	36	56.3	52.6	12.4
Isfahan(32.5N,51.7E)	29	61.1	61.3	11.5
Hongkong(22.3N,114.2E)	47	49.7	50.9	7.8
Hilo(19.4N,155.0W)	58	46.3	50.9	6.8
Alajuela(10.0N,84.2W)	27	40.7	40.5	4.2
Heredia(10.0N,84.1W)	16	40.7	43.5	5.9
Panama(7.8N,80.3W)	2	38.7	44.0	6.5
Kuala(2.7N,101.7E)	51	34.2	35.2	5.6
Sancr(0.9S,89.6W)	31	38.4	36.7	5.0
Nairobi(1.3S,36.8E)	52	37.8	46.2	9.9
Malindi(3.0S,40.2E)	13	45.0	51.3	7.6

Natal(5.4S,35.4W)	58	47.7	49.0	6.0
Java(7.5S,112.6E)	44	35.3	34.8	6.7
Ascen(8.0S,14.4W)	56	50.9	55.2	6.7
Samoa(14.2S,170.6W)	56	31.5	30.8	4.5
Fiji(18.1S,178.4E)	22	34.7	34.2	4.7
Reunion(21.0S,55.5E)	52	50.5	59.9	11.7

547

548

549 **Table 2.** Tropospheric column ozone zonal mean climatology (in Dobson Units) from
550 OMI/MLS at 5° latitude resolution.
551

Latitudes	Jan	Feb	Mar	Apr	May	Jun	Jul	Aug	Sep	Oct	Nov	Dec
60N-65N	35.8	34.6	33.1	33.7	34.3	33.8	33.8	30.7	28.2	27.9	33.8	35.8
55N-60N	33.0	32.2	33.0	33.7	34.6	35.6	35.5	32.9	29.5	28.1	30.3	33.6
50N-55N	31.1	32.1	32.9	33.5	35.2	36.7	36.9	34.7	30.8	28.4	28.8	30.1
45N-50N	29.4	30.8	31.6	33.7	35.9	38.2	39.1	37.4	33.2	28.9	27.9	28.0
40N-45N	27.6	28.9	30.9	34.1	37.0	40.9	42.2	40.7	35.7	30.2	27.3	27.3
35N-40N	27.0	27.7	30.9	35.2	38.9	43.0	44.0	42.3	37.9	32.4	28.4	27.3
30N-35N	28.2	28.6	32.9	38.0	41.2	42.9	42.3	40.4	37.3	33.5	30.9	29.0
25N-30N	30.2	31.6	35.9	40.5	42.0	39.8	38.3	36.8	35.0	33.1	31.9	30.6
20N-25N	31.6	32.4	36.9	40.5	40.4	37.1	35.3	33.6	33.0	32.0	31.7	31.6
15N-20N	31.1	31.3	35.2	38.0	37.1	34.3	32.0	30.0	29.8	29.7	30.2	31.0
10N-15N	29.2	29.3	32.7	34.1	32.6	30.3	28.2	26.8	27.3	27.7	28.6	29.5
5N-10N	27.2	27.6	29.9	29.8	27.7	26.5	25.8	25.1	26.1	26.3	26.6	27.7
0-5N	25.2	25.5	26.8	26.0	24.9	25.3	25.8	26.4	27.2	26.9	26.4	26.4
0-5S	24.4	24.0	24.8	24.1	25.0	26.9	27.5	28.7	30.1	29.9	28.5	26.9
5S-10S	24.2	22.9	23.4	23.5	25.4	27.8	28.5	30.0	32.0	32.3	30.4	27.7
10S-15S	24.5	23.0	23.6	23.9	26.0	28.7	29.5	30.8	33.3	33.9	32.1	28.7
15S-20S	26.6	24.7	24.8	25.2	27.1	29.8	31.0	32.5	35.5	36.4	34.2	30.5
20S-25S	29.8	27.9	27.6	27.6	28.7	30.9	32.7	35.1	38.2	39.5	37.3	33.5
25S-30S	32.4	30.6	29.9	29.3	29.8	31.4	34.2	36.8	40.2	41.2	39.3	36.2

30S-35S	33.9	31.8	30.5	28.6	28.3	30.0	33.4	36.2	38.9	39.5	37.5	35.9
35S-40S	32.2	30.4	28.4	26.4	26.2	27.6	30.7	33.9	35.4	35.0	32.5	31.7
40S-45S	28.0	27.2	26.0	25.6	25.6	26.5	28.5	30.5	31.6	30.3	28.3	27.1
45S-50S	25.6	25.8	25.7	25.9	25.8	25.9	26.7	28.2	30.6	29.9	28.0	25.8
50S-55S	25.3	26.5	27.8	27.5	27.8	29.7	28.5	28.0	31.4	30.7	28.4	25.4
55S-60S	23.6	26.5	28.4	26.8	28.6	28.5	29.4	28.8	30.2	29.5	26.7	23.7
60S-65S	22.6	25.8	27.5	26.6	29.8	33.2	33.6	28.3	27.0	31.2	25.8	22.0

552

553

554 **Table 3.** Global stratospheric column ozone zonal mean climatology (in Dobson Units)
555 derived from MLS integrated ozone profiles at 5° latitude resolution.
556

Latitudes	Jan	Feb	Mar	Apr	May	Jun	Jul	Aug	Sep	Oct	Nov	Dec
85N-90N	311	350	352	340	324	297	269	253	243	246	267	279
80N-85N	314	363	361	359	330	300	269	252	244	251	270	281
75N-80N	319	363	363	359	330	301	272	254	248	254	275	287
70N-75N	326	359	361	359	333	303	275	262	256	259	279	293
65N-70N	330	359	359	355	332	304	280	269	262	265	280	299
60N-65N	333	359	359	352	331	306	286	274	267	269	283	306
55N-60N	332	355	354	347	329	307	291	277	270	270	282	309
50N-55N	329	349	348	340	325	306	290	276	267	267	279	308
45N-50N	321	338	338	331	318	299	280	269	262	260	273	302
40N-45N	307	320	324	318	304	286	266	259	254	252	265	289
35N-40N	284	292	300	298	286	271	256	252	248	243	252	269
30N-35N	257	262	272	275	269	259	251	248	244	237	237	247
25N-30N	234	238	248	255	256	252	248	246	242	234	229	230
20N-25N	221	224	234	242	246	246	245	244	240	232	224	219
15N-20N	215	218	227	235	240	242	244	245	241	232	223	215
10N-15N	214	216	224	232	237	240	244	245	242	232	223	214
5N-10N	215	217	223	230	234	237	240	242	240	231	224	216
0-5N	219	221	226	231	232	233	236	238	237	229	225	219

0-5S	223	224	228	231	230	229	230	233	233	228	225	222
5S-10S	225	226	228	229	227	224	225	228	230	228	227	225
10S-15S	227	227	227	227	223	221	223	226	230	229	230	228
15S-20S	228	226	226	225	222	222	225	228	234	234	233	230
20S-25S	228	225	225	225	224	226	230	235	242	241	239	232
25S-30S	229	226	227	228	229	234	239	248	254	251	247	237
30S-35S	232	230	231	233	239	249	255	267	271	267	259	243
35S-40S	238	235	236	240	250	265	275	288	292	287	274	252
40S-45S	248	242	241	247	259	276	290	303	308	304	288	263
45S-50S	260	250	247	255	267	282	298	310	316	313	298	273
50S-55S	269	257	252	259	270	282	294	305	314	313	302	280
55S-60S	275	262	257	262	271	278	281	284	290	299	299	283
60S-65S	274	264	258	261	269	273	264	247	242	271	283	280
65S-70S	269	261	257	256	263	264	247	211	186	233	254	273
70S-75S	264	257	257	250	254	253	235	198	150	196	224	267
75S-80S	259	253	252	242	247	244	226	196	135	173	205	260
80S-85S	258	252	246	237	238	237	225	202	134	147	190	256
85S-90S	252	246	237	230	237	236	225	204	135	142	187	252

570
571
572
573
574
575
576
577
578
579
580
581
582
583
584
585
586
587
588
589 **Figures**
590

OMI/MLS and Ozonesondes in the Tropics

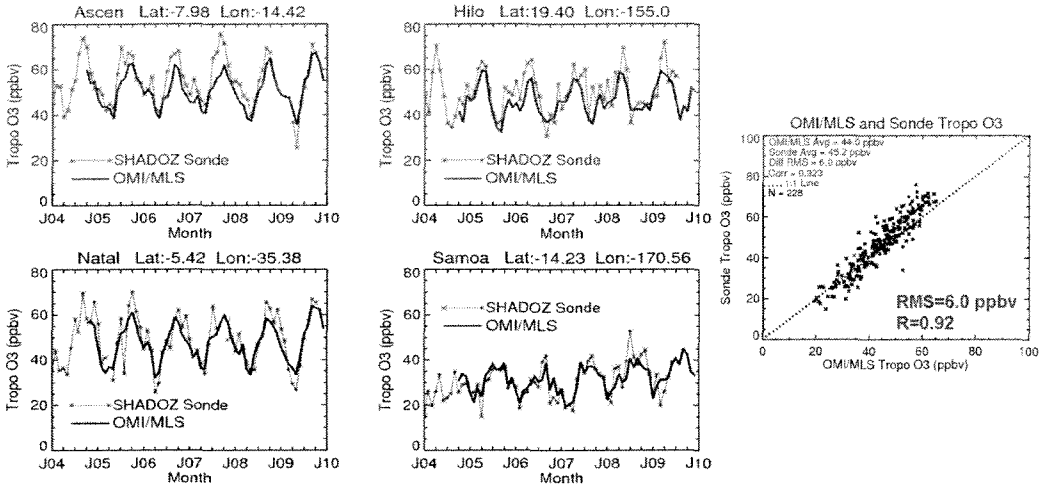

591

592 **Figure 1.** Comparison time series of tropospheric ozone mean volume mixing ratio (in
593 ppbv) between OMI/MLS (dark curves) and several selected common station
594 measurements from SHADOZ (light curves). Also included at far right is a 1-1
595 comparison scatter plot for the measurements.
596
597

OMI/MLS and Ozonesondes in the Extra-Tropics

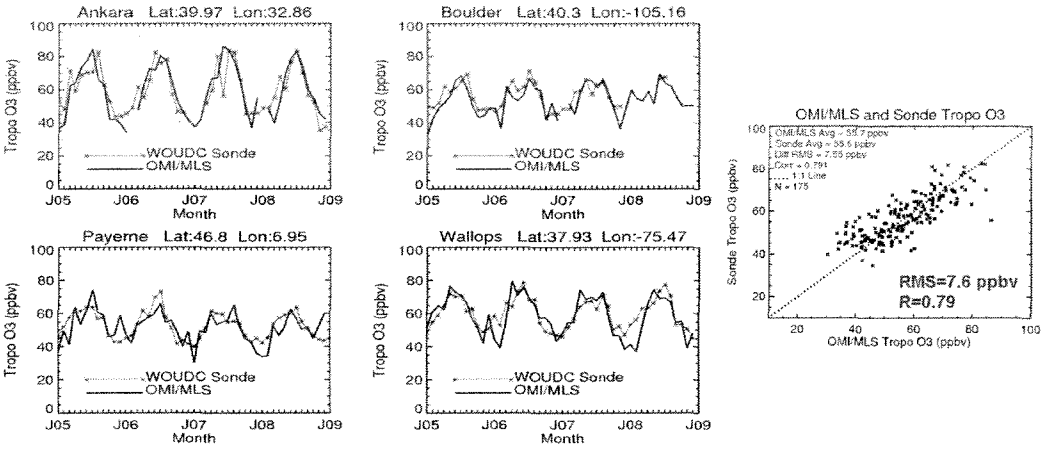

598

599 **Figure 2.** Similar to Figure 1 but for selected extra-tropical WOUDC ozonesonde
600 stations.
601
602

603

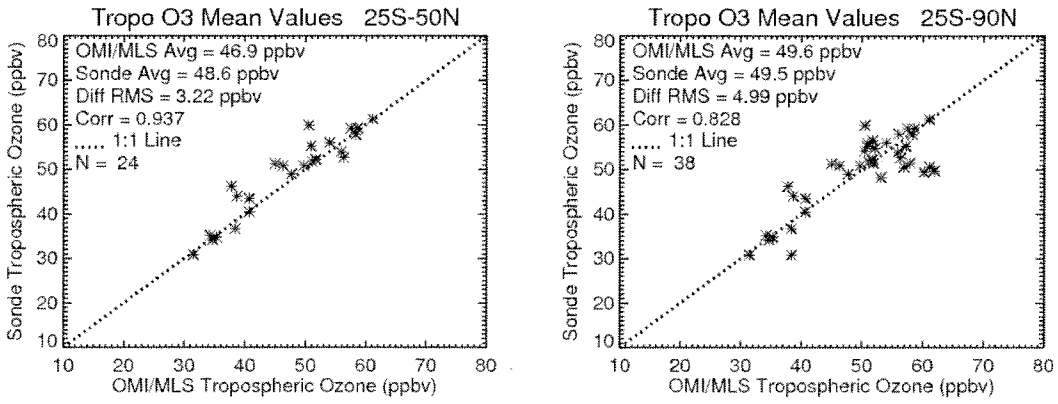

604

605 **Figure 3.** (left) Scatter plots of ozonesonde versus OMI/MLS mean tropospheric ozone
606 for ozonesonde station locations lying between 25°S and 50°N (right) Same as left panel,
607 except for extended latitude range 25°S to 90°N. The values plotted are time series
608 averages in units ppbv.
609
610

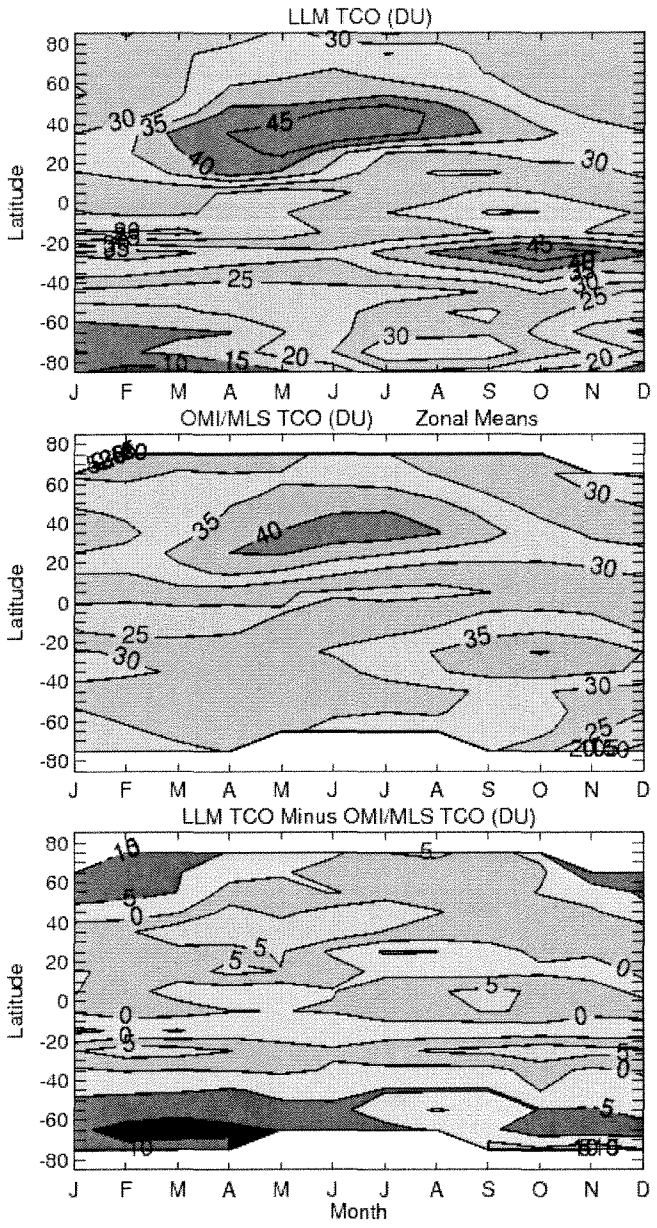

611
612 **Figure 4.** (top) Labow-Logan_McPeters (LLM) tropospheric column ozone climatology.
613 (middle) OMI/MLS tropospheric column ozone climatology. (bottom) LLM minus
614 OMI/MLS climatology difference. All measurements are in Dobson Units. The colors in
615 the panels going from blue/black to red represent smallest to largest (or most positive)
616 values, respectively.
617
618

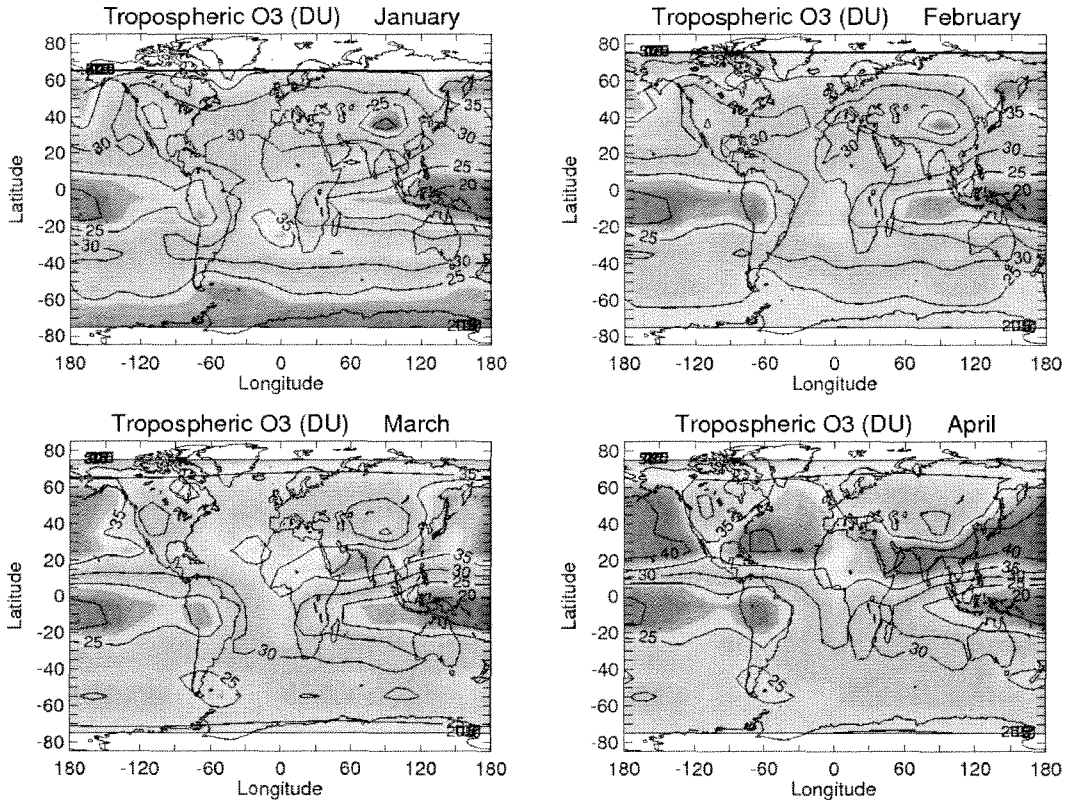

619

620 **Figure 5a.** Tropospheric column ozone climatology (in Dobson Units) for the months
621 January-April from OMI/MLS residual ozone measurements. The colors in the panels
622 going from blue to red represent smallest to largest values, respectively.
623

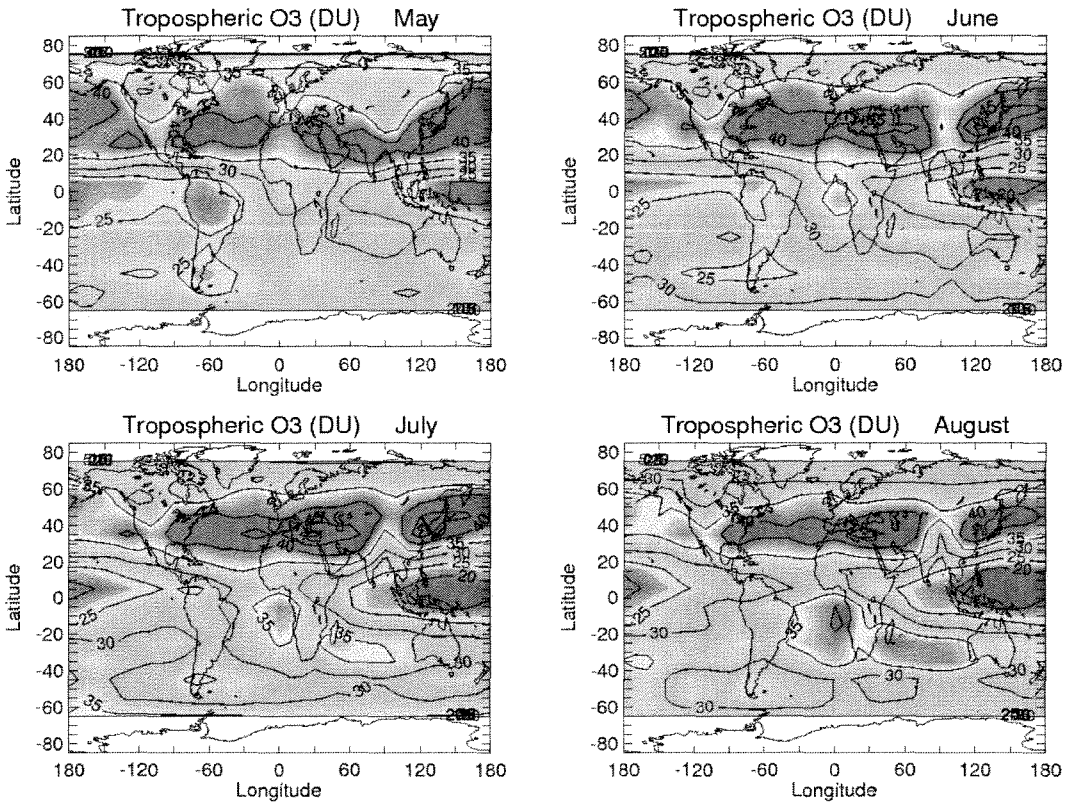

Figure 5b. Same as Figure 5a but for months May-August.

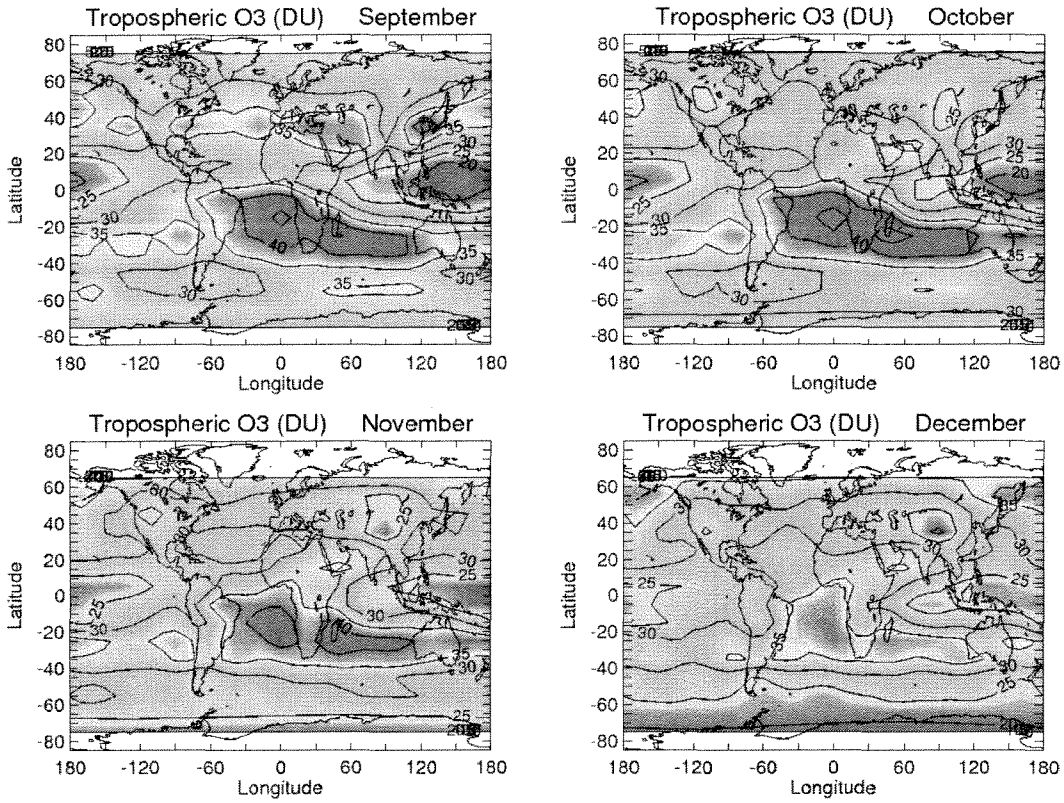

627

628 **Figure 5c.** Same as Figure 5b but for months September-December.

629

630

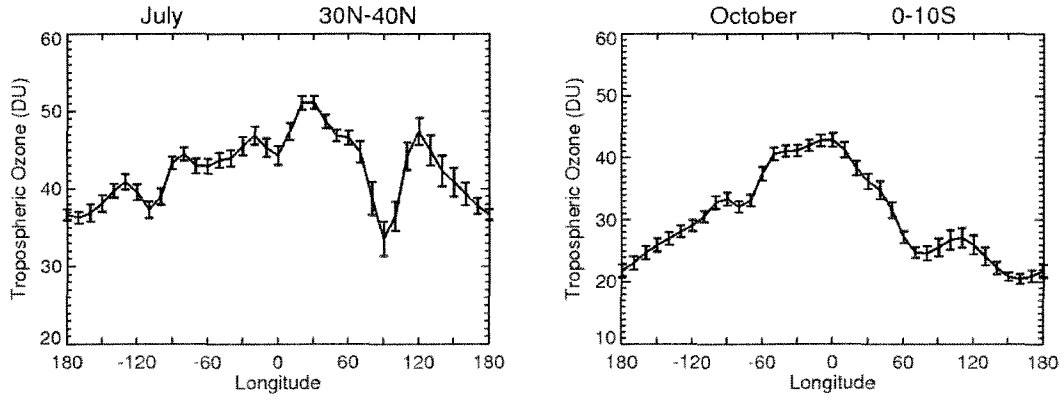

631

632 **Figure 6.** Line plots of tropospheric column ozone (in Dobson Units) as a function of
633 longitude for the latitude bands 30°-40°N and 0°-10°S. The plots include ±2σ
634 uncertainties for illustration where σ is the calculated standard RMS error of the mean.
635
636

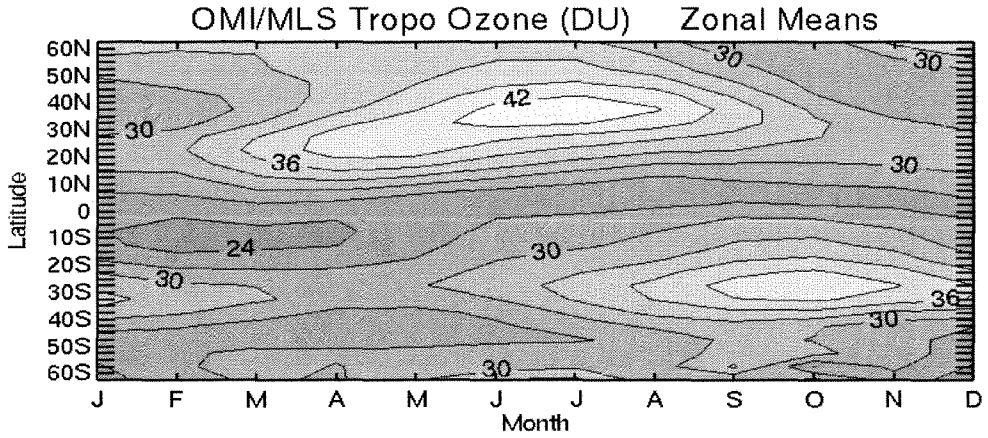

637
638 **Figure 7.** Zonal mean climatology of tropospheric column ozone (in Dobson Units)
639 derived from October 2004 – December 2010 OMI/MLS at 5° latitude resolution. The
640 shading going from dark to light represents smallest to largest values, respectively.
641
642

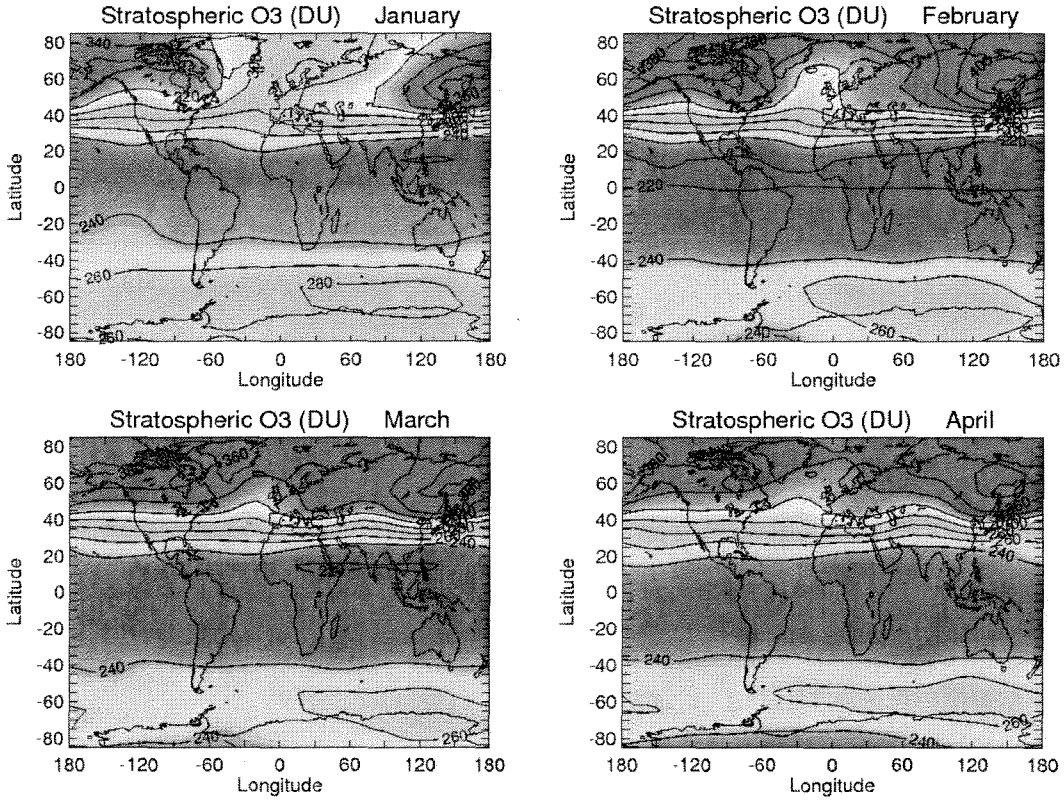

643
644 **Figure 8a.** Similar to Figure 5a but for stratospheric column ozone (in Dobson Units).
645 The colors in the panels going from blue to red represent smallest to largest values,
646 respectively.
647

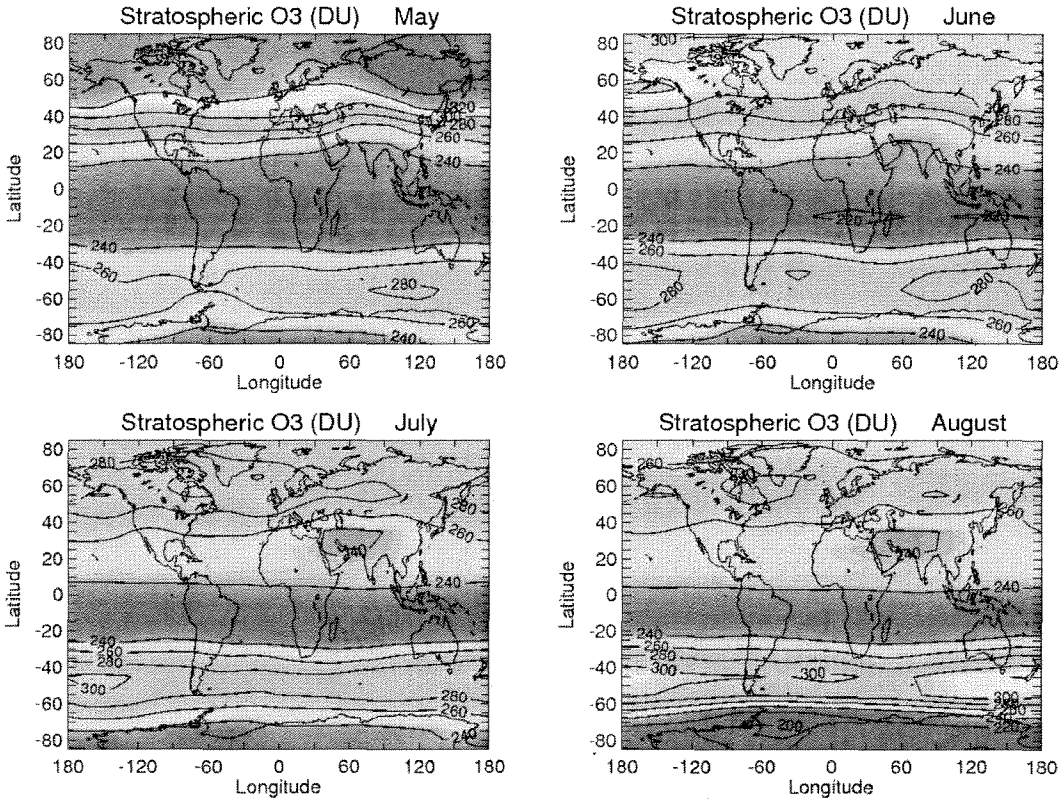

Figure 8b. Similar to Figure 5b but for stratospheric column ozone (in Dobson Units).

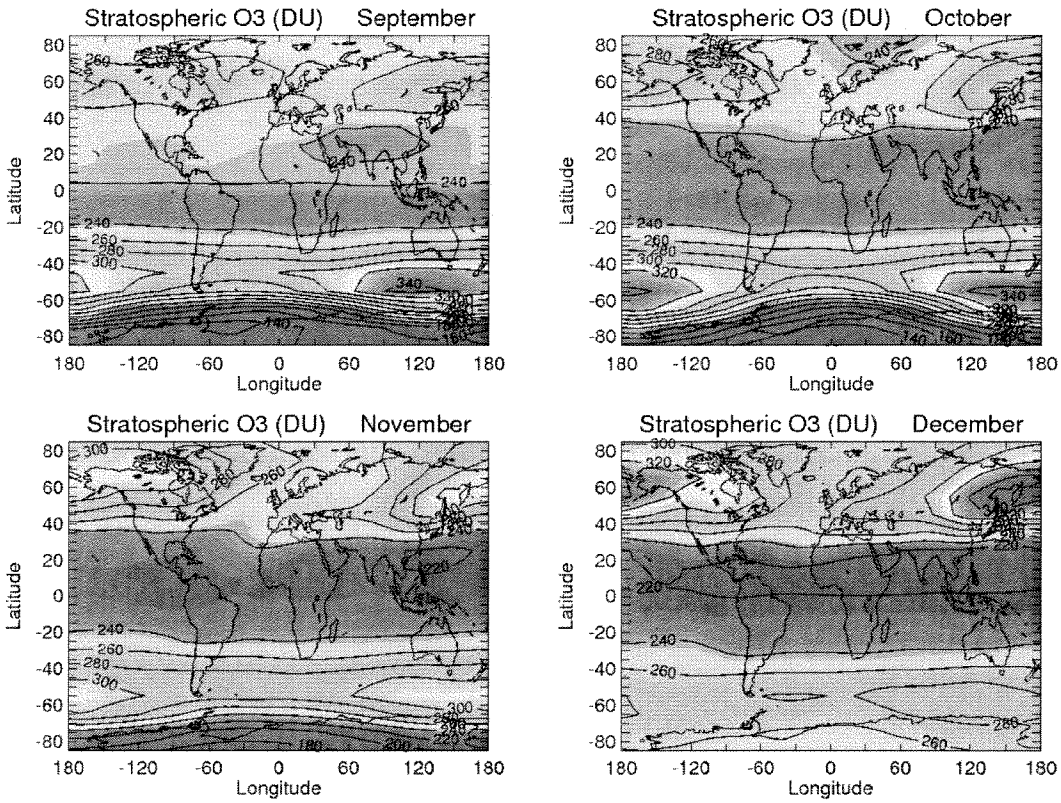

651

652 **Figure 8c.** Similar to Figure 5c but for stratospheric column ozone (in Dobson Units).

653

654

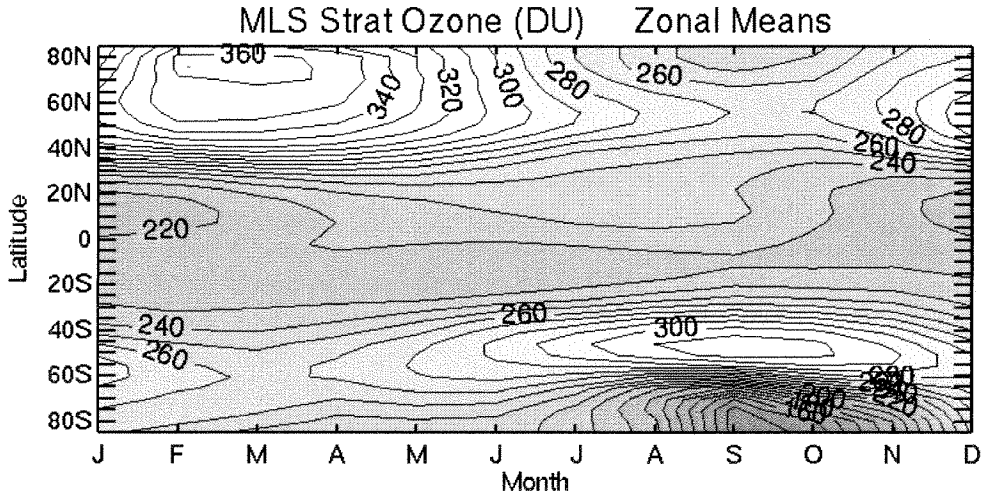

655

Figure 9. Zonal mean climatology of stratospheric column ozone (in Dobson Units) from October 2004 – December 2010 MLS at 5° latitude resolution. The shading going from dark to light represents smallest to largest values, respectively.